



## Removal of cadmium and lead from aqueous solutions by magnetic acid-treated activated carbon nanocomposite

Abbass Jafari Kang, Majid Baghdadi\*, Alireza Pardakhti

Graduate Faculty of Environment, Department of Environmental Engineering, University of Tehran, Tehran, Iran, Tel. +989380777063; email: [abbass.kang@ut.ac.ir](mailto:abbass.kang@ut.ac.ir) (A. Jafari Kang), Tel. +98 21 61112778; Fax: +98 21 66407719; email: [m.baghdadi@ut.ac.ir](mailto:m.baghdadi@ut.ac.ir) (M. Baghdadi), Tel. +98 21 61113587; email: [alirezap@ut.ac.ir](mailto:alirezap@ut.ac.ir) (A. Pardakhti)

Received 28 February 2015; Accepted 11 September 2015

### ABSTRACT

In this study, a new approach was developed for the preparation of magnetic activated carbon (MAC) in which a nanocomposite with the mass ratio of 1:8 ( $\text{Fe}_3\text{O}_4$ :AC) was prepared using commercial activated carbon (AC) treated with nitric acid and magnetite nanoparticles synthesized by co-precipitation method. The MAC was characterized by scanning electron microscopy, nitrogen adsorption isotherm at 77 K, vibrating sample magnetometer, X-ray diffraction, and Fourier transform infrared spectroscopy. The results showed that MAC had desirable magnetic properties and pure  $\text{Fe}_3\text{O}_4$  nanoparticles were successfully synthesized and added to AC. The nanocomposite was successfully used as a separable adsorbent for removing  $\text{Pb}^{2+}$  and  $\text{Cd}^{2+}$  from aqueous solutions. The adsorption performances were evaluated by Langmuir and Freundlich isotherms, which showed the data were well fitted to the Langmuir model. The adsorbent showed good adsorption capacities of 49.8 and 86.2 mg/g for cadmium and lead at the initial pH levels of 6.0 and 5.0, respectively. Kinetic studies were performed using pseudo-first-order and pseudo-second-order kinetic models and the results demonstrated that the adsorption process followed second-order model. Thermodynamics of the adsorption of lead and cadmium onto MAC was also studied with results that showed the adsorption process was endothermic and spontaneous. Adsorption performance of MAC was also evaluated using battery manufacture wastewater samples and removal efficiencies of 91.4 and 96.6% were obtained for the removal of  $\text{Cd}^{2+}$  and  $\text{Pb}^{2+}$ , respectively.

*Keywords:* Magnetic activated carbon; Separable adsorbent;  $\text{Fe}_3\text{O}_4$ ; Heavy metals; Nanocomposite

### 1. Introduction

Drinking water contamination is a worldwide health concern, which has become increasingly important since the 1990s [1]. In recent years, investigation of water contamination with heavy metals has become

the prime focus of environmental scientists [2]. Heavy metal water contamination mainly occurs by natural processes like weathering, erosion of bed rocks, and ore deposits, and anthropogenic processes like mining, smelting, industries, agriculture, and wastewater irrigation [3]. Heavy metals present in some industrial wastewaters, such as pulp and paper, tanneries, petrochemicals, refineries, fertilizers, and steel and

\*Corresponding author.

automobile industries have toxic effects on the receiving environment [4,5]. These metals are transported by runoff water and contaminate water sources downstream from the industrial site [6]. Among various metal ions, lead, mercury, cadmium, and chromium (VI) are at the top level on the toxicity list [7]. Even at low concentrations, these metals can be toxic to organisms including humans [8].

Although the clinical presentations of toxicosis from different metals may be quite varied, most metals induce damage through similar mechanisms, either by binding the metals to vital enzymes or by substituting the metals for other elements in biochemical reactions [9]. Lead is known to damage the kidney, liver, reproductive system, basic cellular processes, and brain functions [10]. A variety of syndromes, renal function hypertension, hepatic injury, lung damage, and teratogenic effects may result from cadmium toxicity [11].

Although various methods, including chemical precipitation [12], ion exchange [13], coagulation and flocculation [14], flotation [15], ultrafiltration [16], nanofiltration [17], reverse osmosis [18], electrodialysis [19], electrocoagulation [20], electroflotation [21], and electrodeposition [22] have been applied for the removal of heavy metals, adsorption is considered one of the major techniques due to flexibility in design, ease of operation, low-cost maintenance, and high efficiency [23,24].

Despite the existence of a significant number of adsorbents for heavy metal removal such as agricultural waste material [25], plant wastes [26], montmorillonite [27], lignin [28], diatomite [29], clino-pyrrhotite [30], lignite [31], aragonite shells [32], natural zeolites [33], clay [34], kaolinite [35], and peat [36], commercial activated carbon (AC) is widely used today.

Powdered AC used for water contaminant uptake has been traditionally discarded with the process sludge after use, which results in secondary pollution [37]. Therefore, it is necessary to use a method of purification that does not generate secondary waste and involves materials that can be recycled and easily used on an industrial scale [38]. In order to solve this problem, magnetic separation as a rapid and effective technology has attracted attention. Combinations of magnetic properties of iron oxides with adsorption properties of carbon nanotube [39], graphene [40], chitosan [41], zeolite [42], mesoporous silica [43], SiO<sub>2</sub> shell [44], and AC [45] have been used for removing different metallic ions.

In recent studies, magnetic activated carbon (MAC) has been developed in two ways. The first method consists of a series of preparation steps start-

ing from AC impregnated with Fe<sup>3+</sup> solution, which is followed by drying and calcination under inert atmosphere [46]. The magnetic composite prepared in this way has been used for removing arsenate [45], methyl orange [47,48], methylene blue [49], and malachite green [50] from aqueous solutions. In the other procedure, AC is added to the solution of Fe<sup>3+</sup> and Fe<sup>2+</sup> salts with the molar ratio of 2:1. Then, co-precipitation of ferric and ferrous ions onto the carbon surface is achieved by adding NaOH or NH<sub>3</sub> to the mixture. The reaction can be expressed as follows [51]:



The magnetic composite developed by this method has been used for removing trinitrophenol [52], cobalt, copper [53], mercury [54], congo red [51], and volatile organic compounds (i.e. phenol, chloroform, and chlorobenzene) [55] from aqueous solutions.

In the previous works, synthesis of magnetite was performed at the presence of AC, which could lead to the formation of other species of iron oxide such as maghemite (magnetic) and hematite (non-magnetic). In the present study, MAC with the weight ratio of Fe<sub>3</sub>O<sub>4</sub>:AC = 1:8 was prepared. In order to avoid the formation of other types of iron oxides, synthesis of Fe<sub>3</sub>O<sub>4</sub>/AC nanocomposite was performed in two separated steps: first, the Fe<sub>3</sub>O<sub>4</sub> magnetic nanoparticles were synthesized by co-precipitation method under inert atmosphere and gathered using a magnet. Second, the magnetite nanoparticles were mixed with the HNO<sub>3</sub>-treated AC suspension. The nanocomposite was used as a high-capacity adsorbent for removing cadmium and lead from the aqueous solutions.

## 2. Experimental

### 2.1. Reagents and equipment

A commercial AC (Loba Chemie, India) with the particle size of 100–200 mesh, nitric acid 65%, iron salts (FeCl<sub>2</sub>·4H<sub>2</sub>O and FeCl<sub>3</sub>·6H<sub>2</sub>O), and ammonia solution 25% (Merck, Germany) was used for preparing the adsorbent. Standard stock solutions (1,000 mg/L) were prepared by dissolving an appropriate amount of Pb(NO<sub>3</sub>)<sub>2</sub> and Cd(NO<sub>3</sub>)<sub>2</sub>·4H<sub>2</sub>O (Merck, Germany) in deionized distilled water. The initial pH of the solutions was adjusted using 0.1 N HCl and 0.1 N NaOH. An atomic absorption spectrophotometer (GBC, 903, USA) was also used for determining metal ions. For the pH adjustments, a pH meter (Metrohm, 691, Switzerland) was applied.

## 2.2. Preparing MAC

In order to obtain a surface modified AC, acid treatment was performed using nitric acid. For this purpose, 20 g of AC was added to 100 ml of HNO<sub>3</sub> (65%). The mixture was constantly stirred for 3 h at 80°C. The nitric acid-treated activated carbon (NAC) was filtered, rinsed, and finally, dried in an oven at 50°C for 24 h. Magnetic Fe<sub>3</sub>O<sub>4</sub>/activated carbon nanocomposite (MAC) with the mass ratio of 1:8 was prepared by the following procedure: Magnetic nanoparticles were synthesized by the co-precipitation of Fe<sup>2+</sup> and Fe<sup>3+</sup> in the absence of atmospheric oxygen. In this step, a 300-ml solution containing 2.92 g of FeCl<sub>3</sub>·6H<sub>2</sub>O and 1.05 g of FeCl<sub>2</sub>·4H<sub>2</sub>O was vigorously stirred at 80°C under the nitrogen flow and 80 ml of ammonia (25%) was added dropwise to the solution for 30 min. Black colloidal magnetic particles were separated by a simple magnetic procedure and rapidly rinsed with 100 ml of deoxygenized water followed by suspension in 500 ml of water. Then, 10 g of NAC was added to the suspension and the mixture was stirred under N<sub>2</sub> flow at room temperature for 1 h. Due to the opposite charges, acid-treated activated carbon (pH<sub>pzc</sub> = 2) and magnetite (pH<sub>pzc</sub> = 6) attract each other at pH range of 2–6, after 1 h mixing, AC adsorbed the nanoparticles. The magnetic composite was easily separated by a magnet, dried at 50°C overnight, and finally, dried at 110°C for 4 h. In order to remove some of the iron ions loaded on the composite surface, the MAC was washed with 500 ml of 0.2 N HCl and then 500 ml of 0.1 N NaOH followed by drying at room temperature.

## 2.3. Characterizing MAC

The point of zero charge (pH<sub>pzc</sub>) for MAC was determined according to the following method: 0.1 M NaCl solutions at different pH values (ranging from 1.0 to 11.0) were prepared using 0.1 N HCl and 0.1 N NaOH. 0.2 g of MAC was added to 20 ml of each solution. The mixtures were stirred for 20 h and the final pH was measured. pH<sub>pzc</sub> was determined as the pH of the NaCl solution that did not change after contact with MAC [48].

Fourier transform infrared spectra (4,000–500 cm<sup>-1</sup>) were recorded on an Fourier transform infrared spectroscopy (FT-IR) spectrometer (Bruker, Tensor 27, Germany) to observe the functional groups of the adsorbent.

The X-ray diffraction (XRD) measurements were carried out on an XRD diffractometer (Bruker, D8 advance, Germany, wavelength of 1.890 Angstrom, Co K<sub>α</sub>, voltage of 40 kW, current of 40 mA).

Surface area and pore distribution were measured by PHS 1020 (PHS, China) surface area analyzer using nitrogen adsorption–desorption method. In order to remove moisture, the samples were initially purged with N<sub>2</sub> gas at 150°C for 2 h.

Surface morphology of the AC and MAC was observed using field emission scanning electronic microscopy (Hitachi, S4160, Japan). The samples were coated with a thin layer of gold and mounted on a copper stab using a double stick carbon stab.

A vibrating sample magnetometer (VSM) (Lake Shore, 7400, USA) was used for magnetization measurements and the hysteresis loop was obtained in a magnetic field at room temperature.

## 2.4. Adsorption experiments

Adsorption studies for cadmium and lead removal were performed using batch experiments. A fixed amount of adsorbent was added to 50 ml of metal solution with varying concentrations from 10 to 200 mg/L. The initial pH of the solutions was set to its optimum value. The solutions were stirred (150 rpm) at room temperature for 1 h to achieve the equilibrium. The adsorbent was separated by a magnet. The metal uptake  $q_e$  (mg/g) can be calculated as Eq. (2):

$$q_e \text{ (mg/g)} = \frac{(C_0 - C_e)V}{W} \quad (2)$$

where  $C_0$  and  $C_e$  are concentrations of the initial and equilibrium metal ions (mg/L),  $V$  is volume of the solution (L), and  $W$  is mass of MAC (g). The influence of different parameters such as initial pH, adsorbent dosage, and NaCl was also studied. For each experimental run, a known amount of the adsorbent was added to 50 ml of metal solution with the definite concentration of 100 mg/L. The initial pH of the solutions was adjusted to the desired values.

The kinetic studies were carried out as follows. For each metal, 500 ml of solution containing metal ions at the concentration of 100 mg/L was stirred at 150 rpm at room temperature. MAC was introduced into the reaction tank at zero time and 10 ml of the solution phase was withdrawn at various time intervals.

## 2.5. Desorption experiments

The reversibility of adsorption was investigated by carrying out adsorption and desorption experiments. First, adsorption of Cd<sup>2+</sup> and Pb<sup>2+</sup> from 50 ml of metal solutions with an initial concentration of 10 mg/L was

performed. After reaching the equilibrium, the adsorbent was separated from the solution and added to a jar containing 50 ml of 0.2 N HCl, followed by stirring for 2 h. The adsorbent then was removed from the solution, washed by deionized water and used for the next cycle.

### 3. Results and discussion

#### 3.1. Characterizing MAC

##### 3.1.1. Point of zero charge of MAC

$\text{pH}_{\text{pzc}}$  is defined as the pH at which the total surface charge of the MAC particles is zero. At the pH levels higher than the  $\text{pH}_{\text{pzc}}$ , the MAC surface is negatively charged, while the surface charge is positive at pH below the  $\text{pH}_{\text{pzc}}$  [56]. The results showed that the  $\text{HNO}_3$  treatment significantly reduced the  $\text{pH}_{\text{pzc}}$  of the AC. The  $\text{pH}_{\text{pzc}}$  was 2.0 for MAC and 6.5 for AC. Thus, MAC is an acidic carbon. Acidic carbons have higher density of oxygen-containing functional groups (such as carboxyls, carbonyls, phenols, lactones, and quinones) which significantly influence adsorption properties and reactivity of ACs [52].

##### 3.1.2. FTIR spectrometry

The FTIR spectra of AC, NAC, and MAC are shown in Fig. 1(a). The FTIR bands can be divided into three ranges of spectra: 4,000–2,000 (usually assigned to dehydration and aliphatic units, mostly free O–H, hydrogen bonded O–H, absorbed  $\text{H}_2\text{O}$ , symmetric and asymmetric stretching in C–H,  $-\text{CH}_2$ , or  $\text{CH}_3$  bonds), 2,000–1,300 (comprising the most

important oxygen functionalities characterized by the presence of C–O and N–O containing structures), and 1,300–800  $\text{cm}^{-1}$  (usually assigned to various C–O single bonds such as those in ethers, phenols, and hydroxyl groups) [57]. Here, absorbance bands around 3,440, 1,680, 1,600, 1,440, 1,120, and 640  $\text{cm}^{-1}$  were observed. The broad absorption band at 3,440  $\text{cm}^{-1}$  corresponds to the hydroxyl (–OH) group [58,59]. The peak around 1,680  $\text{cm}^{-1}$  was assigned to C=O vibrations [59,60]. The C=O stretching vibration of carboxyl acid groups existing in an aromatic ring structure generally appears at 1,700–1,680  $\text{cm}^{-1}$  [61]. The band in the region of 1,600  $\text{cm}^{-1}$  is assigned to C=C aromatic [59,62]. The band observed around 1,440  $\text{cm}^{-1}$  can be ascribed to carboxyl–carbonates structures [63,64]. Also, the absorbance band at 1,120  $\text{cm}^{-1}$  indicates the presence of both hydroxyl and ether-type C–O structures [52]. A strong band at 640 was observed in the spectra of MAC sample indicating the presence of iron oxides [52]. Comparison of the FTIR spectra of AC, NAC, and MAC samples indicated that  $\text{HNO}_3$  treatment increased acidic functional groups at the surface of AC and also, iron oxide nanoparticles were successfully loaded on the adsorbent surface.

##### 3.1.3. X-ray diffraction

Fig. 1(b) shows XRD pattern for the MAC sample. The peaks observed at  $2\theta = 30.17^\circ$ ,  $35.46^\circ$ ,  $43.38^\circ$ ,  $53.69^\circ$ ,  $57.23^\circ$ , and  $62.77^\circ$  correspond to (2 2 0), (3 1 1), (4 0 0), (4 2 2), (5 1 1), and (4 4 0) Bragg reflection, respectively, compared with JCPDS file (No. 65-3107). Therefore, the results confirmed the presence of pure  $\text{Fe}_3\text{O}_4$  with a cubic spinel structure in the MAC

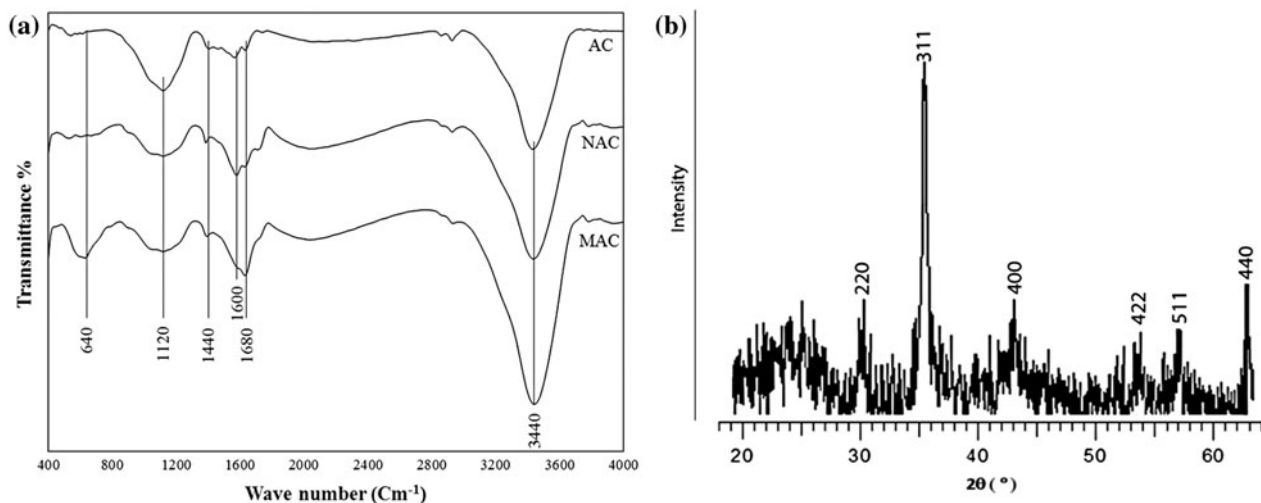


Fig. 1. FTIR spectra of AC, NAC, and MAC (a) and XRD of MAC (b).

sample. Besides, a broad peak centered about  $2\theta = 25^\circ$  was observed corresponding to the AC.

### 3.1.4. Specific surface area and pore volume

The specific surface area, pore volume, and average pore diameter of the AC and MAC were determined by BET method, the results of which are listed in Table 1. Results showed that the preparation procedure reduced both total pore volume and specific surface area of the AC while increasing the average pore diameter. Although no changes were observed in the micropore volume, the mesopore volume decreased by about 10%, which can be explained by the pore blockage caused by the magnetite nanoparticles. Furthermore, the specific surface area of the AC decreased from 1,378 to 1,257 m<sup>2</sup>/g (by less than 9%) due to the occupation of oxygen functional groups and magnetite nanoparticles into porous structure of MAC; hence decreasing the specific surface area [47,52]. Besides, widening of the pore diameters (transformation of some mesopores to macropores) due to the erosive effect of HNO<sub>3</sub> was reported elsewhere [65,66]. As reported, an increase in average pore diameter results in the decrease in BET surface area [67].

### 3.1.5. Field emission scanning electron microscopy (FE-SEM)

Morphology of AC, MAC, and magnetite nanoparticles was investigated by FE-SEM, as shown in Fig. 2. Comparison between scanning electron microscopy (SEM) images of AC (Fig. 3(a)) and MAC (Fig. 3(b)) demonstrated the distortion of porous structure and formation of large macropores due to acid treatment. In a similar study, the formation of porous structure containing very large macropores due to the erosive effect of HNO<sub>3</sub> was reported [66]. As represented in Fig. 3(c), Fe<sub>3</sub>O<sub>4</sub> nanoparticles could be distinguished from the AC, because the former appeared to be brighter than the supporting surface. According to the results, the size of the Fe<sub>3</sub>O<sub>4</sub> nanoparticles attached to the carbon surface was about 44 nm.

### 3.1.6. Vibrating sample magnetization

The magnetization curve of MAC shown in Fig. 3 was obtained by a VSM with an applied magnetic field of 9 KOe at room temperature. The saturation magnetization was 5.06 emu/g for the MAC. These results indicated that the MAC was superparamagnetic (zero coercive field and zero remnant magnetization), which implied uniform and small size of Fe<sub>3</sub>O<sub>4</sub> nanoparticles in the composite [47].

Saturation magnetization of other MACs with different mass ratios of Fe<sub>3</sub>O<sub>4</sub>:AC reported in other works is presented in Table 2. Considering the amount of Fe<sub>3</sub>O<sub>4</sub> used in MAC preparation, the MAC synthesized in this study has a high saturation magnetization. As a matter of fact, at higher ratios of Fe<sub>3</sub>O<sub>4</sub>/AC, greater amounts of active sites of AC are occupied by nanoparticles and consequently, a lower contaminant uptake is achieved. In addition, by using lower amounts of Fe<sub>3</sub>O<sub>4</sub> in MAC preparation, we were able to minimize the preparation costs.

## 3.2. Adsorption studies

### 3.2.1. Effect of pH on the adsorption capacity of MAC

Batch equilibrium studies at various pH levels ranging from 2 to 7 were performed in order to establish the effect of pH on the adsorption of Pb<sup>2+</sup> and Cd<sup>2+</sup> and determine the optimum pH values. Plot of adsorption capacity vs. initial pH for Cd<sup>2+</sup> and Pb<sup>2+</sup> adsorption is given in Fig. 4, demonstrating that the adsorption capacity of MAC toward the metal ions increases with an increase in the initial pH of the solution. The pH of the solution plays a significant role in metal sorption due to the competition of hydrogen ions with metal ions for the sorption sites of the adsorbent. As the pH of solution decreases, the concentration of hydrogen ions increases, which leads to the competitive adsorption between H<sup>+</sup> and the metal ions [68]. Furthermore, pH has an important effect on the surface charge of MAC. As the results showed, the p*H*<sub>pzc</sub> of MAC was 2, meaning that the surface charge of MAC becomes negative at pH greater than 2. Therefore, higher pH favors the adsorption of metals

Table 1  
Specific surface area and pore volume of AC and MAC

	Specific surface area (m <sup>2</sup> /g)	Total pore volume (cm <sup>3</sup> /g)	Micropore volume (cm <sup>3</sup> /g)	Mesopore volume (cm <sup>3</sup> /g)	Average pore diameter (nm)
AC	1,378	0.603	0.0861	0.517	0.561
MAC	1,257	0.549	0.0862	0.463	0.656

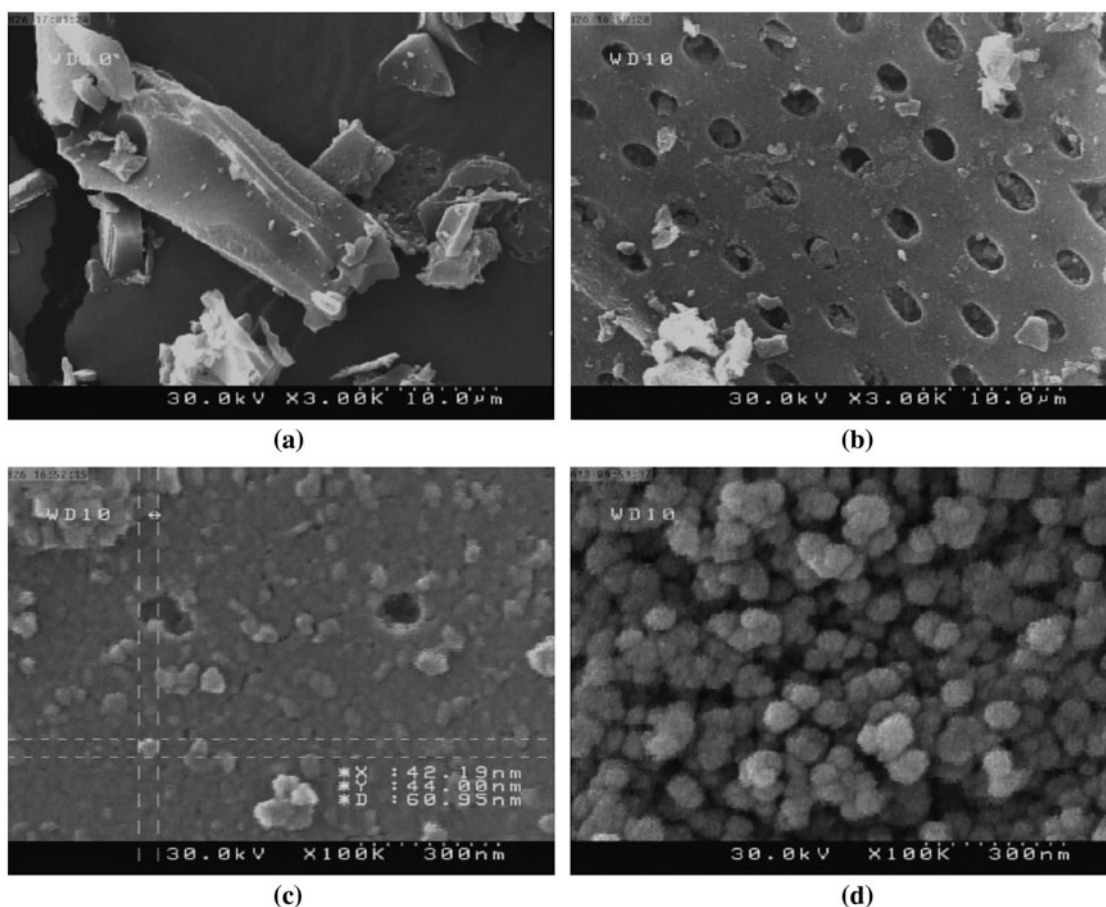


Fig. 2. FESEM of AC  $\times$  3.00 k (a), MAC  $\times$  3.00 k (b), MAC  $\times$  100 k (c), and magnetite nanoparticles  $\times$  100 k (d).

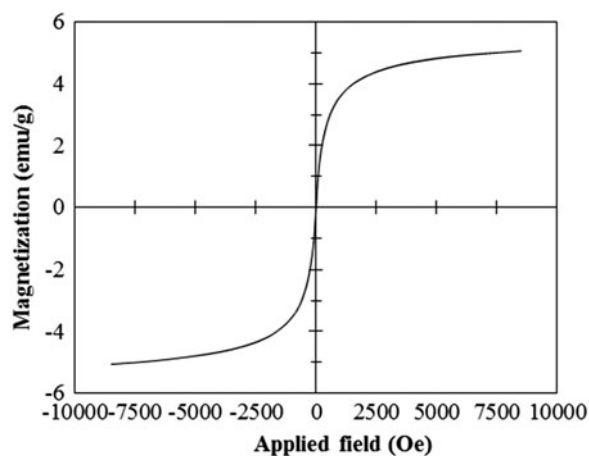


Fig. 3. Magnetization of MAC at 25°C.

onto the MAC surface due to electrostatic attraction. As pH of the solution decreases, the adsorbent surface charge becomes positive and hinders the binding of

the metal ions [69]. Another factor influencing the effect of pH on the adsorption process is cadmium or lead species [70]. According to the speciation diagram reported for  $\text{Cd}^{2+}$  [71], at a pH greater than 6.0, different species of cadmium are formed in aqueous systems; also, the hydrolysis of  $\text{Pb}^{2+}$  occurs at a pH higher than 5.3 [72,73]. Therefore, predominant species of cadmium and lead are  $\text{Cd}^{2+}$  and  $\text{Pb}^{2+}$  at pH lower than 6.0 and 5.3, respectively. In this study, all further experiments for  $\text{Cd}^{2+}$  and  $\text{Pb}^{2+}$  adsorption were performed at pH of 6.0 and 5.0, respectively.

### 3.2.2. Effect of MAC dose and concentration of metal ions

The influence of MAC dosage on the removal efficiency and adsorption capacity of MAC was studied at MAC concentrations of 0.2–1.6 g/L. As shown in Fig. 5(a), for both  $\text{Cd}^{2+}$  and  $\text{Pb}^{2+}$ , the removal efficiency increased with the increase in the adsorbent dosage, while the adsorption capacity decreased. This

Table 2  
Magnetic properties of MACs at different ratios of Fe<sub>3</sub>O<sub>4</sub>

	Present study	Zang et al. [37]			Yang et al. [49]	Mohan et al. [52]	Do et al. [47]		
Fe <sub>3</sub> O <sub>4</sub> (wt %)	11.1	33	40	50	23	15.4	5	10	30
emu/g	5.06	0.97	2.30	5.93	2.78	4.47	0.3	4.7	7

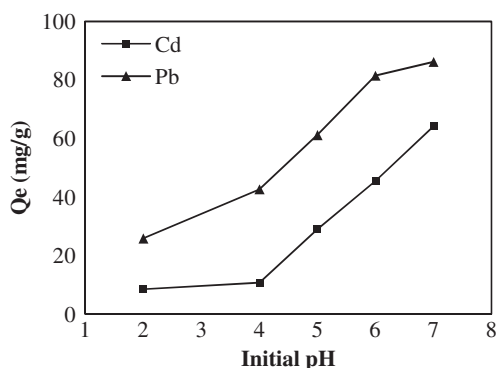


Fig. 4. Effect of pH on the adsorption of Cd<sup>2+</sup> and Pb<sup>2+</sup> onto MAC (initial concentration 100 mg/L, MAC dose of 0.4 g/L).

can be explained by the fact that greater amount of active sites are available at higher dosage of the adsorbent [74]. Maximum uptake of Cd<sup>2+</sup> and Pb<sup>2+</sup> ions by MAC at the adsorbent dosage of 0.2 g/L was found to be 48.7 and 84.5 mg/g, respectively. Therefore, further batch experiments were performed with the adsorbent dosage of 0.2 g/L.

Effect of metal concentration on the removal efficiency of MAC was studied for Cd<sup>2+</sup> and Pb<sup>2+</sup> solutions at varying concentrations from 10 to 200 mg/L. It can be seen in Fig. 5(b) that the percentage removal

was decreased with an increase in the initial concentration of metal solutions. At lower initial concentrations of the metal ions, a higher percentage removal was observed, because the ratio of the available active sites on the adsorbent surface to the initial concentration of adsorbate was higher; so, the active sites on the MAC adsorbed most of Cd<sup>2+</sup> and Pb<sup>2+</sup> ions from the solution [75]. At the initial concentration of 10 mg/L, MAC exhibited the highest removal efficiencies of 95.5 and 90% for Cd<sup>2+</sup> and Pb<sup>2+</sup>, respectively.

### 3.2.3. Effect of contact time

The plot of adsorption capacity vs. contact time shown in Fig. 6 indicates that the adsorption of metal ions (Cd<sup>2+</sup> and Pb<sup>2+</sup>) rapidly increased in the first 30 min; thereafter, a constant value of the adsorption capacity was observed over time. Therefore, the equilibrium time was found to be around 30 min. Similar results have been reported by other researchers [59,76,77].

### 3.2.4. Effect of ionic strength

In order to study the effect of ionic strength on the adsorption of Cd<sup>2+</sup> and Pb<sup>2+</sup> onto MAC, adsorption experiments at the presence of different amounts of

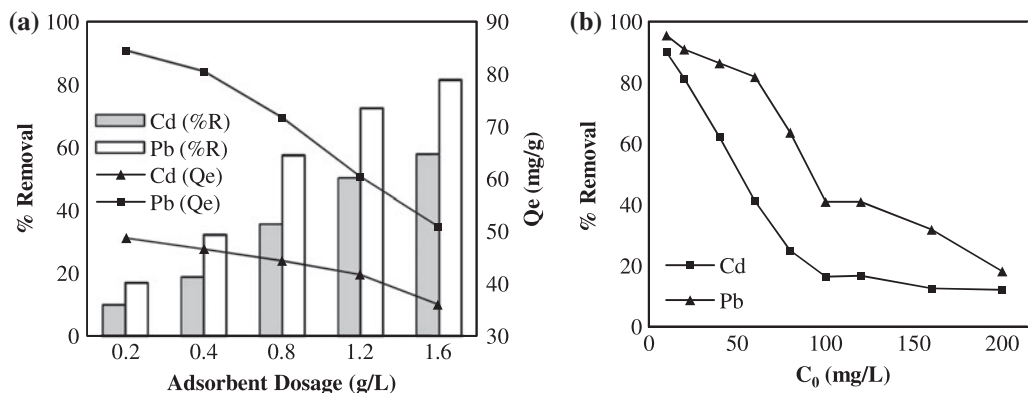


Fig. 5. Effect of (a) MAC dose (initial concentration 50 mg/L) and (b) initial metal concentration (MAC dose of 0.2 g/L) on the adsorption of Cd<sup>2+</sup> (pH<sub>in</sub> 6.0) and Pb<sup>2+</sup> (pH<sub>in</sub> 5.0).

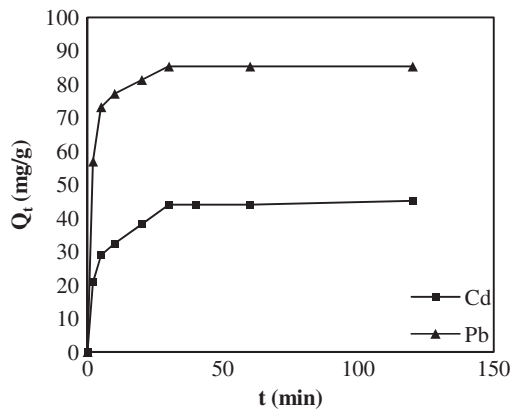


Fig. 6. Effect of contact time on the adsorption of  $\text{Cd}^{2+}$  ( $\text{pH}_{\text{in}} 6.0$ ) and  $\text{Pb}^{2+}$  ( $\text{pH}_{\text{in}} 5.0$ ) onto MAC (initial concentration 100 mg/L, MAC dosage 0.2 g/L).

NaCl ranging from 0 to 5% (0–5,000 mg/g) were conducted. The results shown in Fig. 7 indicate that the adsorption of both  $\text{Cd}^{2+}$  and  $\text{Pb}^{2+}$  ions onto MAC decreased with the increase in the NaCl concentration. Due to the competition of  $\text{Na}^+$  ions with  $\text{Cd}^{2+}$  and  $\text{Pb}^{2+}$  ions to complex with the surface acidic group of the MAC, adsorption of  $\text{Cd}^{2+}$  and  $\text{Pb}^{2+}$  decreased in the presence of  $\text{Na}^+$  ions. On the other hand, formation of more stable  $\text{PbCl}$  and  $\text{Cd-Cl}$  complexes due to the binding of  $\text{Cl}^-$  ions with  $\text{Cd}^{2+}$  and  $\text{Pb}^{2+}$  ions decreased the affinity of the metal ions toward the adsorbent [78,79].

### 3.2.5. Adsorption isotherms

Equilibrium adsorption isotherms are important in determining the adsorption capacity of metal ions and

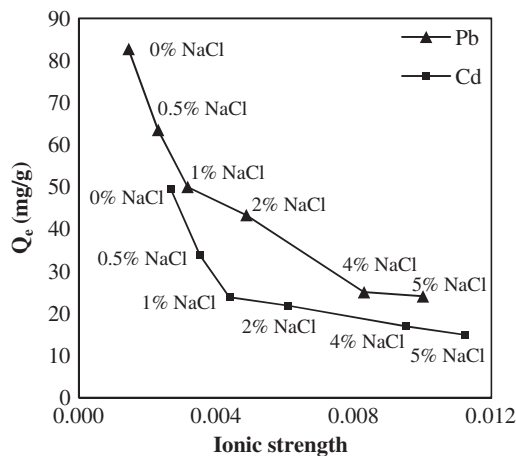


Fig. 7. Effect of ionic strength on the adsorption of  $\text{Cd}^{2+}$  ( $\text{pH}_{\text{in}} 6.0$ ) and  $\text{Pb}^{2+}$  ( $\text{pH}_{\text{in}} 5.0$ ) onto MAC (initial concentration of 100 mg/L, MAC dosage 0.2 g/L).

diagnosing the nature of adsorption onto the adsorbent [80]. Langmuir and Freundlich equations, as the most common models, were used to evaluate the adsorption isotherm. The Langmuir isotherm model assumes a monolayer adsorption which takes place at specific homogeneous sites within the adsorbent and all the adsorption sites are energetically identical [81]. The Langmuir equation is defined as in Eq. (3):

$$q_e = \frac{bQ_0C_e}{1+bC_e} \quad (3)$$

where  $Q_0$  and  $b$  are the characteristic Langmuir parameters,  $Q_0$  is the maximum adsorption capacity that is the amount of metal to form a complete monolayer in mg/g, and  $b$  is a constant related to the intensity of adsorption in L/mg [82]. The Langmuir parameters are achieved by the linearized equation as given in Eq. (4):

$$\frac{C_e}{q_e} = \frac{1}{Q_0b} + \frac{C_e}{Q_0} \quad (4)$$

Essential characteristics of the Langmuir isotherm can be also expressed in terms of a dimensionless constant of separation factor or equilibrium parameter,  $R_L$ , which is defined as Eq. (5):

$$R_L = \frac{1}{1+bC_0} \quad (5)$$

where  $b$  is the Langmuir constant and  $C_0$  is the initial concentration of metal ions. Also, the  $R_L$  value indicates the shape of the isotherm;  $R$  values between 0 and 1 indicate favorable adsorption, while  $R_L > 1$ ,  $R_L = 1$ , and  $R_L = 0$  indicate unfavorable, linear, and irreversible adsorption isotherms, respectively [80].

The Freundlich isotherm is considered for describing both multilayer adsorption and adsorption on heterogeneous surfaces [83] and can be written as in Eq. (6):

$$q_e = \frac{1}{n} K_f C_e \quad (6)$$

where  $q_e$  is the amount of metal ions adsorbed onto the unit mass of adsorbent at equilibrium (mg/g),  $C_e$  is the equilibrium concentration of the metal ions (mg/L), and  $K_f$  and  $n$  are Freundlich constants related to the adsorption capacity and adsorption intensity, respectively [84]. If the value of  $1/n$  is lower than 1, it indicates a normal Langmuir

isotherm [72]. The Freundlich parameters were carried out by the linearized form of the Freundlich equation as given in Eq. (7):

$$\log q_e = \log K_f + \left(\frac{1}{n}\right) \log C_e \quad (7)$$

The Langmuir and Freundlich plots are shown in Fig. 8(a) and (b), respectively. Langmuir and Freundlich parameters for the adsorption of  $\text{Cd}^{2+}$  and  $\text{Pb}^{2+}$  on the MAC are listed in Table 3. The results showed that the adsorption data for both  $\text{Cd}^{2+}$  and  $\text{Pb}^{2+}$  adsorptions were well fitted to the Langmuir model ( $r^2 = 0.9972$  for  $\text{Cd}^{2+}$  and  $0.9991$  for  $\text{Pb}^{2+}$ ). Therefore, a  $\text{Cd}^{2+}/\text{Pb}^{2+}$  monolayer was formed on the MAC surface with a metal complex formation [81]. The values of  $R_L$  for the Langmuir isotherm were between 0 and 1 and the Freundlich constant  $1/n$  was smaller than 1, which indicated favorable adsorption. The maximum adsorption capacities of  $\text{Cd}^{2+}$  and  $\text{Pb}^{2+}$  determined by Langmuir model were 49.8 and 86.2 mg/g, respectively.

Maximum adsorption capacities of AC and NAC for  $\text{Cd}^{2+}$  and  $\text{Pb}^{2+}$  were also determined under the same conditions. The results showed that the maximum adsorption capacities of AC and NAC for  $\text{Cd}^{2+}$  were 6.50 and 60.4 mg/g, respectively, while they were 11.8 and 99.6 for  $\text{Pb}^{2+}$ , respectively. Comparing the capacities of the adsorbents showed that the acid nitric treatment significantly increased the adsorption capacity. Lower  $\text{Cd}^{2+}$  and  $\text{Pb}^{2+}$  adsorption capacities of MAC were observed compared to those obtained for NAC, which can be explained by the fact that the NAC's active sites were occupied by small amounts of iron oxide nanoparticles.

Several studies have been conducted using different types of AC for the adsorption of heavy metals.

Here, comparative information from the studies on  $\text{Cd}^{2+}$  and  $\text{Pb}^{2+}$  removal by adsorption onto AC is given in Table 4. As can be observed, the MAC prepared in this research showed comparable adsorption capacity for the removal of  $\text{Cd}^{2+}$  and  $\text{Pb}^{2+}$  with respect to other types of ACs.

### 3.2.6. Kinetics of adsorption

Understanding the mechanism of metal ion interaction is essential for controlling the adsorption process [99]. To evaluate the kinetic mechanism of adsorption, the pseudo-first-order and pseudo-second-order of common kinetic models were used. The pseudo-first-order model is given by Eq. (8):

$$\log(q_e - q_t) = \log q_e - k_1 \frac{t}{2.303} \quad (8)$$

where  $k_1$  (1/min) is the rate constant for pseudo-first-order adsorption and  $q_e$  and  $q_t$  (mg/g) are the amounts of metal ions adsorbed onto the unit mass of the MAC at equilibrium and at time  $t$  (min), respectively. The pseudo-second-order model is given by Eq. (9):

$$\frac{t}{q_t} = \frac{1}{K_2 q_e^2} + \frac{t}{q_e} \quad (9)$$

where  $k_2$  (g/mg min) is the rate constant for pseudo-second-order adsorption.

Results of the kinetic models are listed in Table 5. The plots shown in Fig. 9(a) and (b) display the first- and second-order models for the adsorption of metal ions onto the MAC, respectively. The pseudo-first-order model was applicable only for the first 30 min at

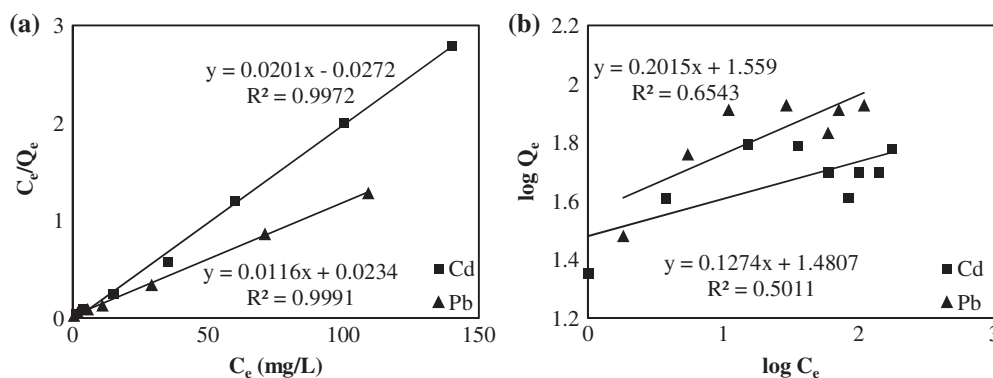


Fig. 8. Langmuir (a) and Freundlich (b) isotherms for the adsorption of  $\text{Cd}^{2+}$  ( $\text{pH}_{\text{in}} 6.0$ ) and  $\text{Pb}^{2+}$  ( $\text{pH}_{\text{in}} 5.0$ ) onto MAC (initial concentration 10–100 mg/L, MAC dosage 0.2 g/L).

Table 3  
Langmuir and Freundlich parameters for the adsorption of Cd<sup>2+</sup> and Pb<sup>2+</sup> onto MAC

	Langmuir constants			Freundlich constants		
	Q <sub>0</sub> (mg/g)	b (L/mg)	r <sup>2</sup>	1/n	K <sub>f</sub>	r <sup>2</sup>
Cd <sup>2+</sup>	49.8	0.827	0.9972	0.1274	30.25	0.5011
Pb <sup>2+</sup>	86.2	0.426	0.9991	0.2015	36.22	0.6543

which rapid adsorption took place. In a similar study, the adsorption data were represented by the first-order model only for the rapid initial phase [59], whereas the data were well represented for the entire adsorption period by the pseudo-second-order model. Comparing the correlation coefficients of the two models, the pseudo-second-order model with much higher values of  $r^2$  (0.9997 for Pb<sup>2+</sup> and 0.9994 for Cd<sup>2+</sup>) can better describe the adsorption kinetics. Also, the equilibrium metal adsorption values calculated ( $q_{cal.}$ ) by the pseudo-second-order model were very close to the experimental values ( $q_{exp.}$ ) compared with the values calculated using the other model.

The adsorption mechanism can be described by three steps of external diffusion (transport of the solute from bulk solution through a liquid film to the adsorbent's exterior surface), intraparticle diffusion (solute diffusion into the pore of the adsorbent), and adsorption reaction (sorption of the solute onto the interior surfaces of the pores and capillary spaces of the adsorbent) which occurs rapidly [84,100]. To determine the diffusion mechanism, the intraparticle diffusion model was tested. The rate equation for intraparticle diffusion can be determined by the following equation:

$$q_t = k_{id}t^{0.5} + c \quad (10)$$

where  $c$  is constant and  $k_{id}$  (mg/g min<sup>0.5</sup>) is the intraparticle diffusion rate constant.

The plot derived from the intraparticle diffusion equation is shown in Fig. 10. The three phases in the intraparticle diffusion plot suggest that the adsorption process proceeds by external diffusion, intraparticle diffusion, and adsorption reaction. In most cases, adsorption occurs rapidly. Therefore, the first two steps are important in the adsorption kinetics [91]. The initial portion of the plot indicates a boundary layer effect. This stage is completed in about 10 min. The second portion (10–30 min) is due to intraparticle diffusion [101,102] and the third portion is the final equilibrium step where the intraparticle diffusion starts to decrease due to less available adsorbent sites

[103]. Slope of the second linear portion of the plot is defined as the intraparticle diffusion rate constant. The intraparticle diffusion parameters are listed in Table 5.

### 3.2.7. Thermodynamics of adsorption

To examine the effect of temperature, adsorption experiments were conducted at 298, 318, and 338 K. It was also found that the adsorption capacities of Cd<sup>2+</sup> and Pb<sup>2+</sup> increased with increasing temperature. Therefore, it can be concluded that the adsorption of the metal ions onto the MAC is an endothermic adsorption process. Thermodynamic parameters such as change in enthalpy ( $\Delta H^\circ$ ), free energy ( $\Delta G^\circ$ ), and entropy ( $\Delta S^\circ$ ) for the adsorption of Cd<sup>2+</sup> and Pb<sup>2+</sup> onto the MAC were calculated using the following equations:

$$K_c = \frac{C_s}{C_e} \quad (11)$$

$$\Delta G^\circ = -RT \ln K_c \quad (12)$$

$$\ln K_c = \frac{\Delta S^\circ}{R} - \frac{\Delta H^\circ}{RT} \quad (13)$$

where  $K_c$  is equilibrium constant,  $C_s$  and  $C_e$  are the concentrations of metal ions on the surface of MAC (mg/g) and in the liquid phase at equilibrium (mg/L),  $R$  is the universal gas constant (8.314 J/mol K), and  $T$  is temperature (K).

$\Delta S^\circ$  and  $\Delta H^\circ$  can be calculated from slope and intercept of Van't Hoff plot of  $\ln K_c$  vs.  $1/T$  (Fig. 11). The thermodynamic parameters are listed in Table 6. Positive values of  $\Delta H^\circ$  indicated that the adsorption processes for both Cd<sup>2+</sup> and Pb<sup>2+</sup> were endothermic [104]. Also, positive values of  $\Delta S^\circ$  showed the affinity of the metal ions and increasing randomness at solid–solution interface during the adsorption process [105]. Negative values of  $\Delta G^\circ$  indicated spontaneous adsorption in which the degree of spontaneity increased with the increase in the temperature [106].

Table 4

Comparative information from some studies on heavy metal adsorption by AC

Activated carbon (AC)	Particle size	Pb <sup>2+</sup> (mg/g)	Cd <sup>2+</sup> (mg/g)	Refs.
AC derived from bagasse	<325 mesh	–	38.3 (pH 4.5)	[85]
AC prepared from coirpith	250–500 μm	–	93.4 (pH 5)	[84]
Chemically-activated carbon prepared by reacting corn stalks with concentrated sulfuric acid at 180–220°C	–	–	36.42 (pH 6)	[59]
AC prepared from coconut shell with sulfuric acid activation	90 μm	26.51 (pH 4.5)	–	[77]
Porous particles composed of curdlan and AC	60–100 mesh	75 (pH 6)	41 (pH 6)	[86]
AC prepared from apricot stone and activated with H <sub>2</sub> SO <sub>4</sub>	1–1.25 mm	22.85 (pH 6)	33.57 (pH 6)	[87]
Commercial AC	10–30 mesh	10.77 (pH 6)	–	[88]
Tannic acid immobilized granular AC	20–60 mesh	–	1.51 (pH 5.7)	[89]
Commercial [palm shell based] AC	0.8–1.0 mm	95.2 (pH 5)	–	[90]
AC prepared from renewable plant material [ <i>Euphorbia rigida</i> ] with H <sub>2</sub> SO <sub>4</sub> activation	<125 μm	279.72 (pH 5)	–	[91]
Granular AC prepared from peanut shell by phosphoric acid activation, modified by HNO <sub>3</sub> [20% by mass]	10–20 mesh	35.5	–	[92]
AC were prepared from Tamarind wood material by chemical activation with sulfuric acid	–	134.22 (pH 6.5)	–	[76]
AC prepared from olive stone activated with ZnCl <sub>2</sub>	150–350 μm	–	1.85 (pH 6.15)	[68]
AC modified with tartrazine	100–150 μm	25.5 (pH 8)	13.2 (pH 8)	[93]
AC prepared from <i>Spartina alterniflora</i> by phosphoric acid activation	0.03–0.08 cm	99 (pH 5.6)	–	[70]
AC prepared from sawdust of rubber wood ( <i>Havea brasiliensis</i> )	80–230 mesh	93.43 (pH 5)	–	[94]
AC prepared from phaseolus aureus hulls	100 mesh	21.8 (pH 6)	15.7 (pH 8)	[80]
Granular AC treated with nitric acid (NGAC) in presence of anionic surfactant of SDS	20–40 mesh	–	NGAC = 18.88(pH 6) SDS = 22.82 (pH 6)	[95]
AC modified by 1-acylthiosemicarbazide	100–200 mesh	48.56 (pH 3)	–	[96]
AC prepared from Tamarind wood with ZnCl <sub>2</sub> activation	<150 μm	43.85 (pH 6.2)	–	[97]
AC impregnated with anionic surfactants	20–40 mesh	–	22.26 (pH 6)	[95]
AC produced from palm kernel shell	1.68–2.38 mm	1.337 (pH 5)	–	[60]
AC prepared from <i>Polygonum orientale</i> Linn with phosphoric acid activation.	160 mesh	98.39 (pH 5)	–	[72]
AC prepared from Apricot stone material by chemical activation with sulfuric acid	125–250 μm	21.38 (pH 6)	–	[69]
AC prepared from the cones of the European Black pine	20 mesh	27.53 (pH 6.7)	–	[98]
AC from lotus stalks by guanidine phosphate activation (GPP) and phosphoric acid activation (PPA)	100–160 mesh	–	33.16 (PPA) 39.45 (GPP)	[63]
Magnetic activated carbon (MAC) prepared by activated carbon (AC) treated with nitric acid (NAC) and Fe <sub>3</sub> O <sub>4</sub> nanoparticles	100–200 mesh	AC = 11.82 NAC = 99.61 MAC = 86.21 (pH 5)	AC = 6.5 NAC = 60.37 MAC = 49.75 (pH 6)	Present study

Table 5  
Kinetic parameter for the adsorption of Cd<sup>2+</sup> and Pb<sup>2+</sup> onto MAC

	Pseudo-first-order				Pseudo-second-order				Intraparticle diffusion		
	Q <sub>exp.</sub> (mg/g)	Q <sub>cal.</sub> (mg/g)	k <sub>1</sub> × 10 <sup>3</sup> (1/min)	r <sup>2</sup>	Q <sub>exp.</sub> (mg/g)	Q <sub>cal.</sub> (mg/g)	k <sub>2</sub> × 10 <sup>3</sup> (g/mg min)	r <sup>2</sup>	K <sub>id</sub> (mg/g min <sup>0.5</sup> )	c	r <sup>2</sup>
Cd <sup>2+</sup>	45.14	25.03	65.41	0.97	45.14	46.29	7.08	0.9994	4.62	18.16	0.9925
Pb <sup>2+</sup>	85.37	25.56	97.65	0.90	85.37	86.20	10.94	0.9997	3.67	65.18	0.9959

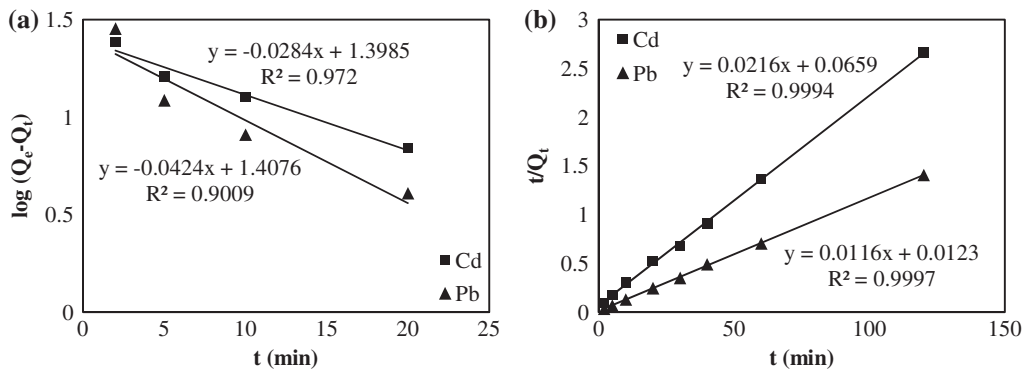


Fig. 9. Pseudo-first-order (a) and pseudo-second-order (b) models for adsorption of Cd<sup>2+</sup> (pH<sub>in</sub> 6.0) and Pb<sup>2+</sup> (pH<sub>in</sub> 5.0) onto MAC (initial concentration of 100 mg/L, MAC dosage 0.2 g/L).

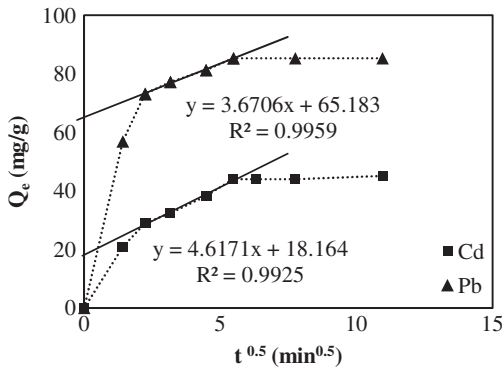


Fig. 10. Intraparticle diffusion model for adsorption of Cd<sup>2+</sup> (pH<sub>in</sub> 6.0) and Pb<sup>2+</sup> (pH<sub>in</sub> 5.0) onto MAC (initial concentration of 100 mg/L, MAC dosage 0.2 g/L).

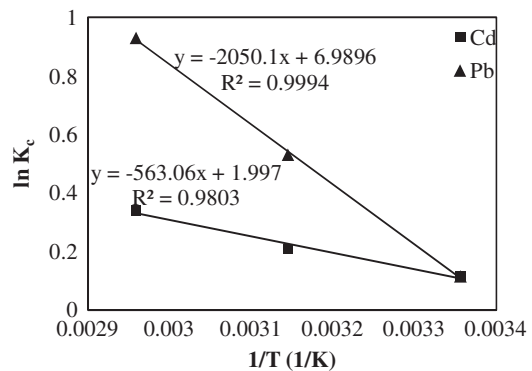


Fig. 11. Van't Hoff plot for adsorption of Cd<sup>2+</sup> (pH<sub>in</sub> 6.0) and Pb<sup>2+</sup> (pH<sub>in</sub> 5.0) onto MAC (initial concentration of 100 mg/L, MAC dosage 0.2 g/L).

### 3.3. Regeneration of MAC

Fig. 12 shows the removal efficiency of MAC from the five cycles. As can be seen, the efficiencies of MAC from the five cycles were 90.5, 89.8, 87.7, 84.2, and 80.5% for Cd<sup>2+</sup> and 95, 93.4, 92, 89.2, and 85.7% for Pb<sup>2+</sup>, respectively. For both Cd<sup>2+</sup> and Pb<sup>2+</sup>,

the results showed no significant decrease in the removal efficiency of MAC from the first to the fifth cycle (11% for Cd and 10% for Pb). It can be concluded that MAC can be recycled to the former condition without any adverse effect on its adsorption characteristics.

Table 6

Thermodynamics parameters for the adsorption of  $\text{Cd}^{2+}$  and  $\text{Pb}^{2+}$  onto MAC

	$\Delta H^\circ$ (kJ/mol)	$\Delta S^\circ$ (J/mol K)	$\Delta G^\circ$ (kJ/mol)		
			298 K	318 K	338 K
$\text{Cd}^{2+}$	8.391	28.313	-0.056	-0.590	-1.191
$\text{Pb}^{2+}$	17.044	58.115	-0.286	-1.405	-2.614

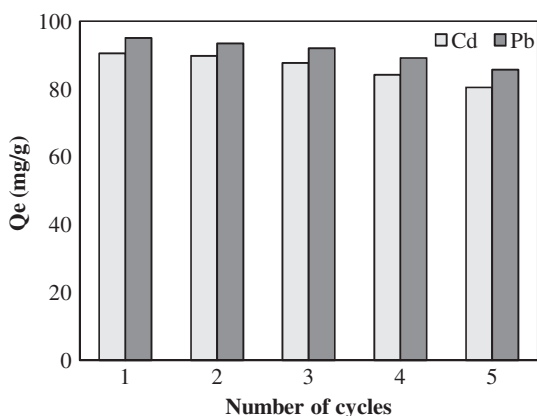


Fig. 12. Adsorption capacity of  $\text{Cd}^{2+}$  ( $\text{pH}_{\text{in}}$  6.0) and  $\text{Pb}^{2+}$  ( $\text{pH}_{\text{in}}$  5.0) onto MAC by multiple cycles of regeneration (Initial concentration of 10 mg/L, MAC dosage 0.2 g/L).

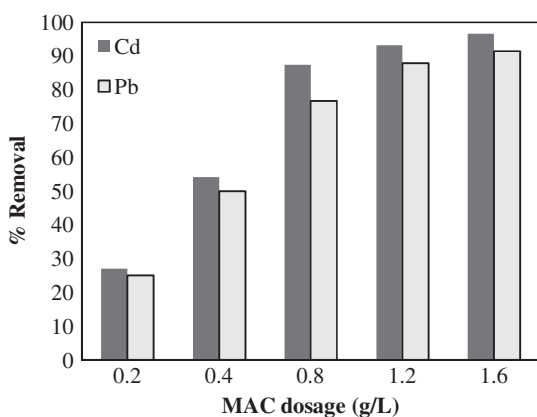


Fig. 13. Removal efficiency of MAC for the removal of  $\text{Cd}^{2+}$  and  $\text{Pb}^{2+}$  from battery wastewater.

#### 3.4. Removal of $\text{Pb}^{2+}$ and $\text{Cd}^{2+}$ from battery manufacture wastewater by MAC

MAC was tested for cadmium and lead removal from battery manufacture wastewater (obtained from Kerman Industrial Park) containing 20.8 mg/L  $\text{Cd}^{2+}$  and 55.5 mg/L  $\text{Pb}^{2+}$  with pH of 5.6. For this aim, different doses of MAC were applied for the removal of  $\text{Pb}^{2+}$  and  $\text{Cd}^{2+}$ . The results shown in Fig. 13 indicate

that at higher doses of the adsorbent, MAC is able to remove greater amounts of  $\text{Cd}^{2+}$  and  $\text{Pb}^{2+}$  from the wastewater. The maximum removal efficiencies of  $\text{Cd}^{2+}$  and  $\text{Pb}^{2+}$  obtained using 1.6 g/L of MAC were 91.4 and 96.6%, respectively.

#### 4. Conclusion

In this study, a MAC with the mass ratio of 1:8 ( $\text{Fe}_3\text{O}_4$ :AC) was successfully produced using a new method and its characterization was performed by different techniques. The MAC was an acidic carbon and the  $\text{pH}_{\text{pzc}}$  was 2.0. The FTIR spectra indicated surface acidic functional groups on the surface of the MAC. The specific surface area of the MAC measured by BET method was 1,257  $\text{m}^2/\text{g}$ . The presence of pure  $\text{Fe}_3\text{O}_4$  with cubic spinel structure at the surface of the MAC was confirmed by XRD analysis. Saturation magnetization of the MAC was 5.06 emu/g, which made it a magnetically separable adsorbent.

The adsorbent was successfully used for removing heavy metals from aqueous solutions. The pH of solution, MAC dosage, initial metal concentration, temperature, contact time, and ionic strength had a significant effect on the heavy metals adsorption capacity of the MAC. The maximum adsorption capacities of cadmium and lead on MAC was 49.8 mg/g at pH 6.0 and 86.2 mg/g at pH 5.0, respectively. Results of isotherm studies showed that the Langmuir model was well fitted with the experimental data. Besides, the pseudo-second-order model could better describe the adsorption kinetics. The thermodynamic parameters of lead and cadmium adsorption onto MAC indicated that the adsorption process was endothermic and spontaneous. Desorption studies showed that MAC could be recycled after the adsorption and used for a minimum of five cycles. The prepared adsorbent was successfully used for the removal of  $\text{Cd}^{2+}$  and  $\text{Pb}^{2+}$  from battery manufacture wastewater with removal efficiencies of 91.4 and 96.6%, respectively.

#### Acknowledgments

This research was supported by Nanotechnology Research Center, Graduate Faculty of Environment,

University of Tehran. The authors wish to acknowledge Jonathan Himelspanch for his contributions to this research.

### List of Symbols

$q_e$	—	adsorption capacity at equilibrium time (mg/g)
$C_0$	—	initial concentration (mg/L)
$C_e$	—	equilibrium concentration (mg/L)
$V$	—	volume (L)
$W$	—	mass (g)
$Q_0$	—	maximum adsorption capacity (mg/g)
$b$	—	Langmuir constant for intensity of adsorption (L/mg)
$R_L$	—	Langmuir constant of separation
$K_f$	—	Freundlich constant of adsorption capacity
$n$	—	Freundlich constant for adsorption intensity
$k_1$	—	rate constant for pseudo-first-order (1/min)
$q_t$	—	adsorbed capacity (mg/g) at time $t$ (min)
$k_2$	—	rate constant for pseudo-second-order (g/mg min)
$k_{id}$	—	intraparticle diffusion rate constant
$K_c$	—	thermodynamic equilibrium constant
$C_s$	—	concentration of metal ions on the surface of adsorbent at equilibrium (mg/g)
$C_e$	—	concentration of metal ions in the liquid phase at equilibrium (mg/l)
$R$	—	universal gas constant (8.314 J/mol K)
$T$	—	temperature (K)

### Abbreviations

AC	—	activated carbon
NAC	—	nitric acid treated activated carbon
MAC	—	magnetic activated carbon

### References

- [1] K. Khan, Y. Lu, H. Khan, S. Zakir, Ihsanullah, S. Khan, A.A. Khan, L. Wei, T. Wang, Health risks associated with heavy metals in the drinking water of Swat, northern Pakistan, *J. Environ. Sci.* 25 (2013) 2003–2013.
- [2] S. Muhammad, M.T. Shah, S. Khan, Health risk assessment of heavy metals and their source apportionment in drinking water of Kohistan region, northern Pakistan, *Microchem. J.* 98 (2011) 334–343.
- [3] M.T. Shah, J. Ara, S. Muhammad, S. Khan, S. Tariq, Health risk assessment via surface water and sub-surface water consumption in the mafic and ultramafic terrain, Mohmand agency, northern Pakistan, *J. Geochem. Explor.* 118 (2012) 60–67.
- [4] M. Yunus Pamukoglu, F. Kargi, Removal of copper (II) ions from aqueous medium by biosorption onto powdered waste sludge, *Process Biochem.* 41 (2006) 1047–1054.
- [5] S.E. Bailey, T.J. Olin, R.M. Bricka, D.D. Adrian, A review of potentially low-cost sorbents for heavy metals, *Water Res.* 33 (1999) 2469–2479.
- [6] N.K. Srivastava, C.B. Majumder, Novel biofiltration methods for the treatment of heavy metals from industrial wastewater, *J. Hazard. Mater.* 151 (2008) 1–8.
- [7] U. Farooq, J.A. Kozinski, M.A. Khan, M. Athar, Biosorption of heavy metal ions using wheat based biosorbents—A review of the recent literature, *Biore-sour. Technol.* 101 (2010) 5043–5053.
- [8] T. Bahadir, G. Bakan, L. Altas, H. Buyukgungor, The investigation of lead removal by biosorption: An application at storage battery industry wastewaters, *Enzyme Microb. Technol.* 41 (2007) 98–102.
- [9] S.M. Gwaltney-Brant, Chapter 41—Heavy metals, in: W.M. Haschek, C.G. Rousseaux, M.A. Wallig (Eds.), *Haschek and Rousseaux's Handbook of Toxicologic Pathology*, Academic Press, Boston, MA, 2013, pp. 1315–1347.
- [10] R. Naseem, S.S. Tahir, Removal of Pb(II) from aqueous/acidic solutions by using bentonite as an adsorbent, *Water Res.* 35 (2001) 3982–3986.
- [11] A. Heidari, H. Younesi, Z. Mehraban, Removal of Ni(II), Cd(II), and Pb(II) from a ternary aqueous solution by amino functionalized mesoporous and nano mesoporous silica, *Chem. Eng. J.* 153 (2009) 70–79.
- [12] M.T. Alvarez, C. Crespo, B. Mattiasson, Precipitation of Zn(II), Cu(II) and Pb(II) at bench-scale using biogenic hydrogen sulfide from the utilization of volatile fatty acids, *Chemosphere* 66 (2007) 1677–1683.
- [13] A. Dąbrowski, Z. Hubicki, P. Podkościelny, E. Robens, Selective removal of the heavy metal ions from waters and industrial wastewaters by ion-exchange method, *Chemosphere* 56 (2004) 91–106.
- [14] A.G. El Samrani, B.S. Lartiges, F. Villiéras, Chemical coagulation of combined sewer overflow: Heavy metal removal and treatment optimization, *Water Res.* 42 (2008) 951–960.
- [15] B.Y. Medina, M.L. Torem, L.M.S. de Mesquita, On the kinetics of precipitate flotation of Cr III using sodium dodecylsulfate and ethanol, *Miner. Eng.* 18 (2005) 225–231.
- [16] J. Landaburu-Aguirre, V. García, E. Pongrácz, R.L. Keiski, The removal of zinc from synthetic wastewaters by micellar-enhanced ultrafiltration: Statistical design of experiments, *Desalination* 240 (2009) 262–269.
- [17] Z.V.P. Murthy, L.B. Chaudhari, Separation of binary heavy metals from aqueous solutions by nanofiltration and characterization of the membrane using Spiegler-Kedem model, *Chem. Eng. J.* 150 (2009) 181–187.
- [18] B.K.C. Chan, A.W.L. Dudeney, Reverse osmosis removal of arsenic residues from bioleaching of refractory gold concentrates, *Miner. Eng.* 21 (2008) 272–278.
- [19] S.K. Nataraj, K.M. Hosamani, T.M. Aminabhavi, Potential application of an electrodialysis pilot plant containing ion-exchange membranes in chromium removal, *Desalination* 217 (2007) 181–190.
- [20] T. Ölmez, The optimization of Cr(VI) reduction and removal by electrocoagulation using response surface methodology, *J. Hazard. Mater.* 162 (2009) 1371–1378.

- [21] M. Belkacem, M. Khodir, S. Abdelkrim, Treatment characteristics of textile wastewater and removal of heavy metals using the electroflotation technique, *Desalination* 228 (2008) 245–254.
- [22] G. Issabayeva, M.K. Aroua, N.M. Sulaiman, Electrodeposition of copper and lead on palm shell activated carbon in a flow-through electrolytic cell, *Desalination* 194 (2006) 192–201.
- [23] B. Pan, B. Pan, W. Zhang, L. Lv, Q. Zhang, S. Zheng, Development of polymeric and polymer-based hybrid adsorbents for pollutants removal from waters, *Chem. Eng. J.* 151 (2009) 19–29.
- [24] S.P. Mishra, V.K. Singh, D. Tiwari, Radiotracer technique in adsorption study: Part XIV. Efficient removal of mercury from aqueous solutions by hydrous zirconium oxide, *Appl. Radiat. Isot.* 47 (1996) 15–21.
- [25] D. Sud, G. Mahajan, M.P. Kaur, Agricultural waste material as potential adsorbent for sequestering heavy metal ions from aqueous solutions—A review, *Bioresour. Technol.* 99 (2008) 6017–6027.
- [26] W.S. Wan Ngah, M.A.K.M. Hanafiah, Removal of heavy metal ions from wastewater by chemically modified plant wastes as adsorbents: A review, *Bioresour. Technol.* 99 (2008) 3935–3948.
- [27] K.G. Bhattacharyya, S.S. Gupta, Adsorption of a few heavy metals on natural and modified kaolinite and montmorillonite: A review, *Adv. Colloid Interface Sci.* 140 (2008) 114–131.
- [28] M. Betancur, P.R. Bonelli, J.A. Velásquez, A.L. Cukierman, Potentiality of lignin from the Kraft pulping process for removal of trace nickel from wastewater: Effect of demineralisation, *Bioresour. Technol.* 100 (2009) 1130–1137.
- [29] G. Sheng, S. Wang, J. Hu, Y. Lu, J. Li, Y. Dong, X. Wang, Adsorption of Pb(II) on diatomite as affected via aqueous solution chemistry and temperature, *Colloids Surf., A: Physicochem. Eng. Aspects* 339 (2009) 159–166.
- [30] A. Lu, S. Zhong, J. Chen, J. Shi, J. Tang, X. Lu, Removal of Cr(VI) and Cr(III) from aqueous solutions and industrial wastewaters by natural clino-pyrrhotite, *Environ. Sci. Technol.* 40 (2006) 3064–3069.
- [31] D. Mohan, S. Chander, Removal and recovery of metal ions from acid mine drainage using lignite—A low cost sorbent, *J. Hazard. Mater.* 137 (2006) 1545–1553.
- [32] S.J. Köhler, P. Cubillas, J.D. Rodríguez-Blanco, C. Bauer, M. Prieto, Removal of cadmium from wastewaters by aragonite shells and the influence of other divalent cations, *Environ. Sci. Technol.* 41 (2007) 112–118.
- [33] R. Apiratikul, P. Pavasant, Sorption of  $\text{Cu}^{2+}$ ,  $\text{Cd}^{2+}$ , and  $\text{Pb}^{2+}$  using modified zeolite from coal fly ash, *Chem. Eng. J.* 144 (2008) 245–258.
- [34] S.A. Al-Jlil, F.D. Alsewilem, Saudi Arabian clays for lead removal in wastewater, *Appl. Clay Sci.* 42 (2009) 671–674.
- [35] X. Gu, L.J. Evans, Surface complexation modelling of Cd(II), Cu(II), Ni(II), Pb(II) and Zn(II) adsorption onto kaolinite, *Geochim. Cosmochim. Acta* 72 (2008) 267–276.
- [36] Z.-R. Liu, L.-M. Zhou, P. Wei, K. Zeng, C.-X. Wen, H.-H. Lan, Competitive adsorption of heavy metal ions on peat, *J. China Univ. Min. Technol.* 18 (2008) 255–260.
- [37] G. Zhang, J. Qu, H. Liu, A.T. Cooper, R. Wu,  $\text{CuFe}_2\text{O}_4$ /activated carbon composite: A novel magnetic adsorbent for the removal of acid orange II and catalytic regeneration, *Chemosphere* 68 (2007) 1058–1066.
- [38] A.-F. Ngomsik, A. Bee, M. Draye, G. Cote, V. Cabuil, Magnetic nano- and microparticles for metal removal and environmental applications: A review, *C.R. Chim.* 8 (2005) 963–970.
- [39] V.K. Gupta, S. Agarwal, T.A. Saleh, Chromium removal by combining the magnetic properties of iron oxide with adsorption properties of carbon nanotubes, *Water Res.* 45 (2011) 2207–2212.
- [40] X. Guo, B. Du, Q. Wei, J. Yang, L. Hu, L. Yan, W. Xu, Synthesis of amino functionalized magnetic graphenes composite material and its application to remove Cr(VI), Pb(II), Hg(II), Cd(II) and Ni(II) from contaminated water, *J. Hazard. Mater.* 278 (2014) 211–220.
- [41] Y.-C. Chang, D.-H. Chen, Preparation and adsorption properties of monodisperse chitosan-bound  $\text{Fe}_3\text{O}_4$  magnetic nanoparticles for removal of Cu(II) ions, *J. Colloid Interface Sci.* 283 (2005) 446–451.
- [42] H. Liu, S. Peng, L. Shu, T. Chen, T. Bao, R.L. Frost, Magnetic zeolite NaA: Synthesis, characterization based on metakaolin and its application for the removal of  $\text{Cu}^{2+}$ ,  $\text{Pb}^{2+}$ , *Chemosphere* 91 (2013) 1539–1546.
- [43] L. Tang, Y. Fang, Y. Pang, G. Zeng, J. Wang, Y. Zhou, Y. Deng, G. Yang, Y. Cai, J. Chen, Synergistic adsorption and reduction of hexavalent chromium using highly uniform polyaniline-magnetic mesoporous silica composite, *Chem. Eng. J.* 254 (2014) 302–312.
- [44] J. Wang, S. Zheng, Y. Shao, J. Liu, Z. Xu, D. Zhu, Amino-functionalized  $\text{Fe}_3\text{O}_4/\text{SiO}_2$  core-shell magnetic nanomaterial as a novel adsorbent for aqueous heavy metals removal, *J. Colloid Interface Sci.* 349 (2010) 293–299.
- [45] Z. Liu, F.-S. Zhang, R. Sasai, Arsenate removal from water using  $\text{Fe}_3\text{O}_4$ -loaded activated carbon prepared from waste biomass, *Chem. Eng. J.* 160 (2010) 57–62.
- [46] M. Schwickardi, S. Olejnik, E.-L. Salabas, W. Schmidt, F. Schuth, Scalable synthesis of activated carbon with superparamagnetic properties, *Chem. Commun.* (2006) 3987–3989.
- [47] M.H. Do, N.H. Phan, T.D. Nguyen, T.T.S. Pham, V.K. Nguyen, T.T.T. Vu, T.K.P. Nguyen, Activated carbon/ $\text{Fe}_3\text{O}_4$  nanoparticle composite: Fabrication, methyl orange removal and regeneration by hydrogen peroxide, *Chemosphere* 85 (2011) 1269–1276.
- [48] T.D. Nguyen, N.H. Phan, M.H. Do, K.T. Ngo, Magnetic  $\text{Fe}_2\text{MO}_4$  (M:Fe, Mn) activated carbons: Fabrication, characterization and heterogeneous Fenton oxidation of methyl orange, *J. Hazard. Mater.* 185 (2011) 653–661.
- [49] N. Yang, S. Zhu, D. Zhang, S. Xu, Synthesis and properties of magnetic  $\text{Fe}_3\text{O}_4$ -activated carbon nanocomposite particles for dye removal, *Mater. Lett.* 62 (2008) 645–647.
- [50] L. Ai, H. Huang, Z. Chen, X. Wei, J. Jiang, Activated carbon/ $\text{CoFe}_2\text{O}_4$  composites: Facile synthesis, magnetic performance and their potential application for

- the removal of malachite green from water, *Chem. Eng. J.* 156 (2010) 243–249.
- [51] H.Y. Zhu, Y.Q. Fu, R. Jiang, J.H. Jiang, L. Xiao, G.M. Zeng, S.L. Zhao, Y. Wang, Adsorption removal of congo red onto magnetic cellulose/Fe<sub>3</sub>O<sub>4</sub>/activated carbon composite: Equilibrium, kinetic and thermodynamic studies, *Chem. Eng. J.* 173 (2011) 494–502.
- [52] D. Mohan, A. Sarswat, V.K. Singh, M. Alexandre-Franco, C.U. Pittman Jr., Development of magnetic activated carbon from almond shells for trinitrophenol removal from water, *Chem. Eng. J.* 172 (2011) 1111–1125.
- [53] K. Pyrzyńska, M. Bystrzejewski, Comparative study of heavy metal ions sorption onto activated carbon, carbon nanotubes, and carbon-encapsulated magnetic nanoparticles, *Colloids Surf., A: Physicochem. Eng. Aspects* 362 (2010) 102–109.
- [54] E.K. Faulconer, N.V.H. von Reitzenstein, D.W. Mazyck, Optimization of magnetic powdered activated carbon for aqueous Hg(II) removal and magnetic recovery, *J. Hazard. Mater.* 199–200 (2012) 9–14.
- [55] L.C.A. Oliveira, R.V.R.A. Rios, J.D. Fabris, V. Garg, K. Sapag, R.M. Lago, Activated carbon/iron oxide magnetic composites for the adsorption of contaminants in water, *Carbon* 40 (2002) 2177–2183.
- [56] A. Rodríguez, J. García, G. Ovejero, M. Mestanza, Adsorption of anionic and cationic dyes on activated carbon from aqueous solutions: Equilibrium and kinetics, *J. Hazard. Mater.* 172 (2009) 1311–1320.
- [57] H.A. Omar, H. Moloukhia, Use of activated carbon in removal of some radioisotopes from their waste solutions, *J. Hazard. Mater.* 157 (2008) 242–246.
- [58] M. Abbas, S. Kaddour, M. Trari, Kinetic and equilibrium studies of cobalt adsorption on apricot stone activated carbon, *J. Ind. Eng. Chem.* 20 (2014) 745–751.
- [59] A. Youssef, T. El-Nabarawy, S. Samra, Sorption properties of chemically-activated carbons: 1. Sorption of cadmium(II) ions, *Colloids Surf., A: Physicochem. Eng. Aspects* 235 (2004) 153–163.
- [60] Y.B. Onundi, A.A. Mamun, M.F.A. Khatib, Y.M. Ahmed, Adsorption of copper, nickel and lead ions from synthetic semiconductor industrial wastewater by palm shell activated carbon, *Int. J. Environ. Sci. Technol.* 7 (2010) 751–758.
- [61] C. Moreno-Castilla, M.V. López-Ramón, F. Carrasco-Marín, Changes in surface chemistry of activated carbons by wet oxidation, *Carbon* 38 (2000) 1995–2001.
- [62] C. Moreno-Castilla, M.A. Ferro-García, J.P. Joly, I. Bautista-Toledo, F. Carrasco-Marín, J. Rivera-Utrilla, Activated carbon surface modifications by nitric acid, hydrogen peroxide, and ammonium peroxydisulfate treatments, *Langmuir* 11 (1995) 4386–4392.
- [63] H. Liu, Q. Gao, P. Dai, J. Zhang, C. Zhang, N. Bao, Preparation and characterization of activated carbon from lotus stalk with guanidine phosphate activation: Sorption of Cd(II), *J. Anal. Appl. Pyrolysis* 102 (2013) 7–15.
- [64] S. Biniak, G. Szymański, J. Siedlewski, A. Świątkowski, The characterization of activated carbons with oxygen and nitrogen surface groups, *Carbon* 35 (1997) 1799–1810.
- [65] V. Strelko Jr., D.J. Malik, Characterization and metal sorptive properties of oxidized active carbon, *J. Colloid Interface Sci.* 250 (2002) 213–220.
- [66] A.-N.A. El-Hendawy, Influence of HNO<sub>3</sub> oxidation on the structure and adsorptive properties of corncob-based activated carbon, *Carbon* 41 (2003) 713–722.
- [67] N.R. Khalili, M. Campbell, G. Sandi, J. Golaś, Production of micro-and mesoporous activated carbon from paper mill sludge: I Effect of zinc chloride activation, *Carbon* 38 (2000) 1905–1915.
- [68] I. Kula, M. Uğurlu, H. Karaoğlu, A. Çelik, Adsorption of Cd(II) ions from aqueous solutions using activated carbon prepared from olive stone by ZnCl<sub>2</sub> activation, *Bioresour. Technol.* 99 (2008) 492–501.
- [69] L. Mouni, D. Merabet, A. Bouzaza, L. Belkhir, Adsorption of Pb(II) from aqueous solutions using activated carbon developed from Apricot stone, *Desalination* 276 (2011) 148–153.
- [70] K. Li, X. Wang, Adsorptive removal of Pb(II) by activated carbon prepared from *Spartina alterniflora*: Equilibrium, kinetics and thermodynamics, *Bioresour. Technol.* 100 (2009) 2810–2815.
- [71] C.K. Ahn, D. Park, S.H. Woo, J.M. Park, Removal of cationic heavy metal from aqueous solution by activated carbon impregnated with anionic surfactants, *J. Hazard. Mater.* 164 (2009) 1130–1136.
- [72] L. Wang, J. Zhang, R. Zhao, Y. Li, C. Li, C. Zhang, Adsorption of Pb(II) on activated carbon prepared from *Polygonum orientale* Linn.: Kinetics, isotherms, pH, and ionic strength studies, *Bioresour. Technol.* 101 (2010) 5808–5814.
- [73] S. Hao, Y. Zhong, F. Pepe, W. Zhu, Adsorption of Pb<sup>2+</sup> and Cu<sup>2+</sup> on anionic surfactant-templated amino-functionalized mesoporous silicas, *Chem. Eng. J.* 189–190 (2012) 160–167.
- [74] P.A. Mangrulkar, S.P. Kamble, J. Meshram, S.S. Rayalu, Adsorption of phenol and o-chlorophenol by mesoporous MCM-41, *J. Hazard. Mater.* 160 (2008) 414–421.
- [75] F. Raji, M. Pakizeh, Study of Hg(II) species removal from aqueous solution using hybrid ZnCl<sub>2</sub>-MCM-41 adsorbent, *Appl. Surf. Sci.* 282 (2013) 415–424.
- [76] C.K. Singh, J.N. Sahu, K.K. Mahalik, C.R. Mohanty, B.R. Mohan, B.C. Meikap, Studies on the removal of Pb(II) from wastewater by activated carbon developed from Tamarind wood activated with sulphuric acid, *J. Hazard. Mater.* 153 (2008) 221–228.
- [77] M. Sekar, V. Sakthi, S. Rengaraj, Kinetics and equilibrium adsorption study of lead(II) onto activated carbon prepared from coconut shell, *J. Colloid Interface Sci.* 279 (2004) 307–313.
- [78] P. Daorattanachai, F. Unob, A. Imyim, Multi-element preconcentration of heavy metal ions from aqueous solution by APDC impregnated activated carbon, *Talanta* 67 (2005) 59–64.
- [79] I.R. Phillips, D.T. Lamb, D.W. Hawker, E.D. Burton, Effects of pH and Salinity on Copper, Lead, and Zinc Sorption Rates in Sediments from Moreton Bay, Australia, *Bull. Environ. Contam. Toxicol.* 73 (2004) 1041–1048.
- [80] M.M. Rao, D. Ramana, K. Sesaiah, M. Wang, S. Chien, Removal of some metal ions by activated carbon prepared from *Phaseolus aureus* hulls, *J. Hazard. Mater.* 166 (2009) 1006–1013.

- [81] L. Bai, H. Hu, W. Fu, J. Wan, X. Cheng, L. Zhuge, L. Xiong, Q. Chen, Synthesis of a novel silica-supported dithiocarbamate adsorbent and its properties for the removal of heavy metal ions, *J. Hazard. Mater.* 195 (2011) 261–275.
- [82] J. Aguado, J.M. Arsuaga, A. Arencibia, M. Lindo, V. Gascón, Aqueous heavy metals removal by adsorption on amine-functionalized mesoporous silica, *J. Hazard. Mater.* 163 (2009) 213–221.
- [83] M. Anbia, A.H. Davijani, Synthesis of L-Cysteine grafted nanoporous carbon (CMK-3) and its use as a new cadmium sorbent, *Chem. Eng. J.* 223 (2013) 899–907.
- [84] K. Kadirvelu, C. Namasivayam, Activated carbon from coconut coirpith as metal adsorbent: Adsorption of Cd(II) from aqueous solution, *Adv. Environ. Res.* 7 (2003) 471–478.
- [85] D. Mohan, K.P. Singh, Single- and multi-component adsorption of cadmium and zinc using activated carbon derived from bagasse—An agricultural waste, *Water Res.* 36 (2002) 2304–2318.
- [86] C.-J. Moon, J.-H. Lee, Use of curdlan and activated carbon composed adsorbents for heavy metal removal, *Process Biochem.* 40 (2005) 1279–1283.
- [87] M. Kobya, E. Demirbas, E. Senturk, M. Ince, Adsorption of heavy metal ions from aqueous solutions by activated carbon prepared from apricot stone, *Biore-sour. Technol.* 96 (2005) 1518–1521.
- [88] M. Machida, M. Aikawa, H. Tatsumoto, Prediction of simultaneous adsorption of Cu(II) and Pb(II) onto activated carbon by conventional Langmuir type equations, *J. Hazard. Mater.* 120 (2005) 271–275.
- [89] A. Üçer, A. Uyanik, Ş. Aygün, Adsorption of Cu (II), Cd (II), Zn (II), Mn(II) and Fe(III) ions by tannic acid immobilised activated carbon, *Sep. Purif. Technol.* 47 (2006) 113–118.
- [90] G. Issabayeva, M.K. Aroua, N.M.N. Sulaiman, Removal of lead from aqueous solutions on palm shell activated carbon, *Biore-sour. Technol.* 97 (2006) 2350–2355.
- [91] Ö. Gerçel, H.F. Gerçel, Adsorption of lead(II) ions from aqueous solutions by activated carbon prepared from biomass plant material of *Euphorbia rigida*, *Chem. Eng. J.* 132 (2007) 289–297.
- [92] T. Xu, X. Liu, Peanut shell activated carbon: Characterization, surface modification and adsorption of Pb<sup>2+</sup> from aqueous solution, *Chin. J. Chem. Eng.* 16 (2008) 401–406.
- [93] L. Monser, N. Adhoum, Tartrazine modified activated carbon for the removal of Pb(II), Cd(II) and Cr(III), *J. Hazard. Mater.* 161 (2009) 263–269.
- [94] K.G. Sreejalekshmi, K.A. Krishnan, T.S. Anirudhan, Adsorption of Pb(II) and Pb(II)-citric acid on sawdust activated carbon: Kinetic and equilibrium isotherm studies, *J. Hazard. Mater.* 161 (2009) 1506–1513.
- [95] C.K. Ahn, Y.M. Kim, S.H. Woo, J.M. Park, Removal of cadmium using acid-treated activated carbon in the presence of nonionic and/or anionic surfactants, *Hydrometallurgy* 99 (2009) 209–213.
- [96] R. Gao, Z. Hu, X. Chang, Q. He, L. Zhang, Z. Tu, J. Shi, Chemically modified activated carbon with 1-acylthiosemicarbazide for selective solid-phase extraction and preconcentration of trace Cu(II), Hg(II) and Pb(II) from water samples, *J. Hazard. Mater.* 172 (2009) 324–329.
- [97] J. Acharya, J.N. Sahu, C.R. Mohanty, B.C. Meikap, Removal of lead(II) from wastewater by activated carbon developed from Tamarind wood by zinc chloride activation, *Chem. Eng. J.* 149 (2009) 249–262.
- [98] M. Momčilović, M. Purenović, A. Bojić, A. Zarubica, M. Randelović, Removal of lead(II) ions from aqueous solutions by adsorption onto pine cone activated carbon, *Desalination* 276 (2011) 53–59.
- [99] S. Ricordel, S. Taha, I. Cisse, G. Orange, Heavy metals removal by adsorption onto peanut husks carbon: Characterization, kinetic study and modeling, *Sep. Purif. Technol.* 24 (2001) 389–401.
- [100] S. Nethaji, A. Sivasamy, G. Thennarasu, S. Saravanan, Adsorption of Malachite Green dye onto activated carbon derived from *Borassus aethiopicum* flower biomass, *J. Hazard. Mater.* 181 (2010) 271–280.
- [101] V. Vadivelan, K.V. Kumar, Equilibrium, kinetics, mechanism, and process design for the sorption of methylene blue onto rice husk, *J. Colloid Interface Sci.* 286 (2005) 90–100.
- [102] K.V. Kumar, V. Ramamurthi, S. Sivanesan, Modeling the mechanism involved during the sorption of methylene blue onto fly ash, *J. Colloid Interface Sci.* 284 (2005) 14–21.
- [103] J.P. Chen, S. Wu, K.-H. Chong, Surface modification of a granular activated carbon by citric acid for enhancement of copper adsorption, *Carbon* 41 (2003) 1979–1986.
- [104] E. Demirbas, N. Dizge, M. Sulak, M. Kobya, Adsorption kinetics and equilibrium of copper from aqueous solutions using hazelnut shell activated carbon, *Chem. Eng. J.* 148 (2009) 480–487.
- [105] S. Shrestha, G. Son, S.H. Lee, T.G. Lee, Isotherm and thermodynamic studies of Zn (II) adsorption on lignite and coconut shell-based activated carbon fiber, *Chemosphere* 92 (2013) 1053–1061.
- [106] H.K. Boparai, M. Joseph, D.M. O'Carroll, Kinetics and thermodynamics of cadmium ion removal by adsorption onto nano zerovalent iron particles, *J. Hazard. Mater.* 186 (2011) 458–465.